Eidgenössische Technische Hochschule Zürich
Swiss Federal Institute of Technology Zurich

Department of Materials Science

Master thesis

Microfluidic flows of rough colloids

Supervisor: Prof. Dr. Lucio Isa

Author: Hasan Emre Baysal

Student ID: 17-938-226

Email: baysalh@student.ethz.ch

Date of submission: 01.05.2020

Abstract

The clogging of particle suspensions in a channel with a constriction is undesired for diverse technological applications. Several studies have focused on the parameters affecting the clogging characteristic such as flow velocity, particle concentration and channel geometries. This clogging can be seen as a local jamming under flow. Studies of shear-thickening suspensions have been focused to pinpoint the origin of such jamming transition. The effect of interparticle interactions, surface morphology and surface chemistry on the shear thickening of particle suspension has been shown in different studies.

In this thesis, the effect of particle surface roughness on the clogging behavior of rough silica particle suspensions is investigated in a microfluidic channel with a constriction. For this purpose, particles with controlled surface roughness are produced. These particles are pumped through the constriction in the microfluidic channel in order to characterize clog formation. The characterization of the clogging events is done by measuring the particle volume fraction and local flow velocity in the channel.

Suspensions of particles with five different roughness are examined in a wide range of velocities and volume fractions. A correlation between the particle surface roughness and clogging events has been observed. The suspensions of particles with rougher surfaces tend to clog at lower flow velocities.

Particle agglomerations in the microfluidic channel have been noticed. The tendency for agglomeration increased with the particle surface roughness.

The results identify surface roughness as a key parameter in triggering the undesired clogging events in the converging channels. Our findings indicate that surface roughness needs to be taken into consideration in the formulation of dense particulate suspensions for applications ranging from 3D printing to ink-jet printing.

1) Introduction

Granular particles in a channel with a constriction may flow continuously, intermittently, or do not flow when a clog occurs along the flow path (Marin et al., 2018). This kind of flow behavior can be observed in different systems across various length scales, such as sand grains flow through a neck of an hourglass (Wu et al., 1993), microfluidic filtration of undesirable particles in a liquid (Bacchin et al., 2011), a flock of sheep entering a barn (Zuriguel et al., 2014) or people evacuating a building (Zuriguel et al., 2014; Helbing et al., 2000). Clogging events may be helpful in some technological applications, such as micro sieving systems (Brans et al., 2006) and biological cell determination (Pang et al., 2015). On the other hand, it is generally detrimental for the performance and life cycle of systems such as micro-engineered systems, transport of blood cells in vesicles (Vermes et al., 1987), oil recovery (Tavakkoli et al., 2015) and ink printers (Fuller et al. 2002). Nonsticking dry particles and particles in suspensions show considerably similar flow behaviors when they flow across a constriction (Marin et al., 2018). A particle suspension flowing in a micro-channel with constriction may clog when jamming occurs at constriction due to high particle loading (Campbell & Haw, 2010) or even when the particle loading is below jamming concentration (Marin et al., 2018; Dressaire & Sauret, 2017). It has been shown that the jamming volume fraction of particle suspensions depends on the interparticle interactions, surface morphology and surface chemistry (Fernandez et al., 2013; Hsu et al., 2018). In this thesis, we investigated the effect of particle surface roughness on the clogging behavior in a microfluidic channel with a constriction. We focus on using colloidal suspensions to model and study the clogging behavior.

Colloid suspensions consist of objects suspended in a liquid. The object size in colloidal suspensions ranges between 1 nm and 1µm. Particles in this size range are considered big enough that the suspending liquid can be considered a continuum and small enough that thermal fluctuations, which cause Brownian motion, are enough to counteract the weight of the particle so that particles randomly move around. Due to these characteristics, colloids have been used for model systems, i.e. to study the phase behavior of atomic systems (Figure 1). A simple colloidal model system can be created by using ideal hard-sphere objects which are identical, infinitely rigid, not overlapping, only elastically interacting particles. For this reason, the phase behavior of the system only depends on the system entropy which is determined by the possible configuration of particles and volume fraction. Free volume entropy and configurational entropy are two components of the system entropy and the competition between these is the main driving force of the phase transition. The system with ideal spherical particles shows liquid-like behavior until 0.494 volume fraction. In between $\phi_F = 0.494$ and $\phi = 0.545$, liquid and crystalline phases coexisted. It starts to behave like a crystal after $\phi_C = 0.545$. The crystallization of particles fails at $\phi_G = 0.58$ and the system forms glass until $\phi = 0.64$. The reason is the crowding of particle limits to explore all possible configurations in the system (non-ergodic). The maximum random closed packing and maximum crystalline packing is reached at $\phi_{RCP} = 0.64$ and $\phi_{CP} = 0.74$, respectively (Isa, 2008). It is also known that polydispersity (Pournin et al., 2007), particle shape (Doney et al., 2004) and surface roughness (Hsu et al., 2018) affect the volume fractions where phase changes happening.

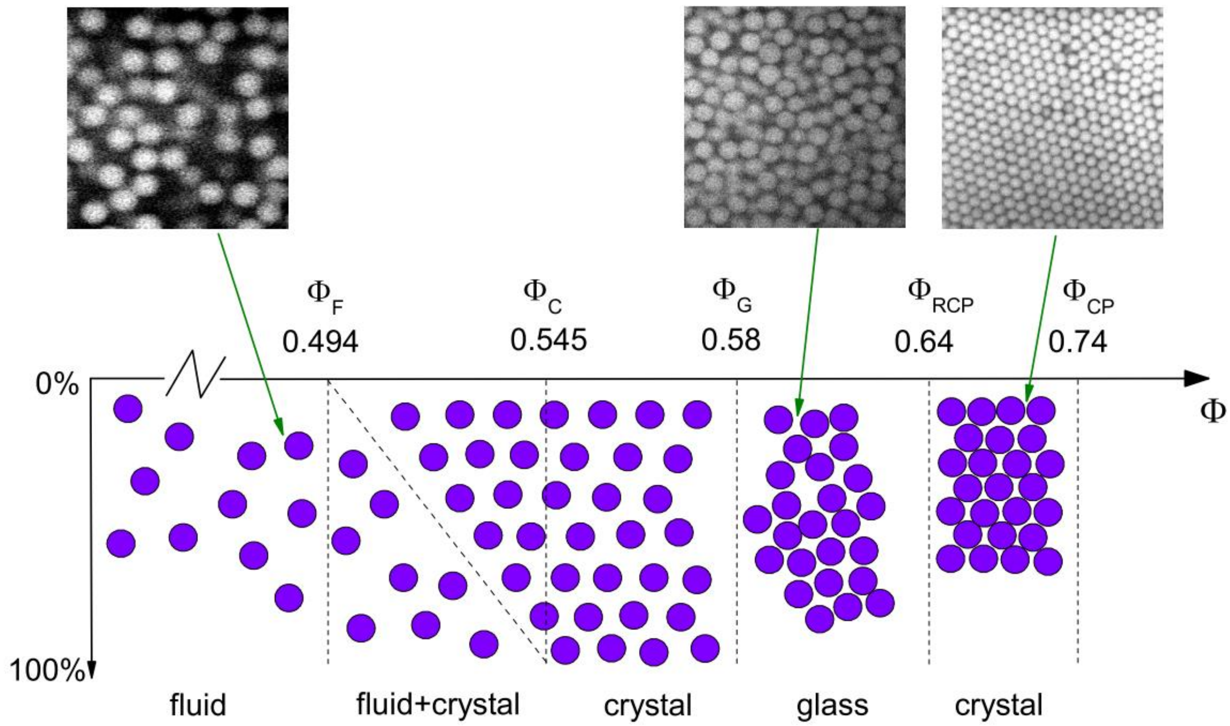

Figure 1 Ideal hard-sphere suspension phase diagram (Isa, 2008).

At volume fractions far lower than the jamming fraction, suspensions behave like a Newtonian fluid and their viscosity is a function of the solvent and particles' volume fraction. When the volume fractions are higher, suspensions display non-Newtonian behaviour, where their viscosity depends also on the applied shear. Above the jamming volume fraction the suspension becomes too dense and the flow stops. The clogging of suspension flow below the jamming fraction, cannot be explained with continuum rheological modeling (Dressaire & Sauret, 2017). However, it can be related to local complex processes. Deposition and assembly of particles in microchannels are associated with these complex local processes which involve hydrodynamic forces, particle morphology and colloidal forces. Sieving, bridging and aggregation are the three clogging mechanisms responsible for the clogging of suspension flow through constricted microchannels (Dressaire & Sauret, 2017). The sieving of rigid particles occurs when the width of constriction is smaller than the particle diameter. It happens mainly due to the size exclusion.

This mechanism makes use of sorting particles with different sizes and gets rid of contaminations in the fluid (Kim et al., 2014). Clogging can also happen with the bridging mechanisms by the formation of bridge-like structures span through the constriction. The particle size is smaller than the constriction width in this mechanism. The formation of arch-like structures is due to the converging flow and high particle concentration in the constriction. Aggregation clogging may occur due to surface properties and therefore particle-particle and particle–wall interactions dominate the dynamics of the clogging behavior (Dressaire & Sauret, 2017).

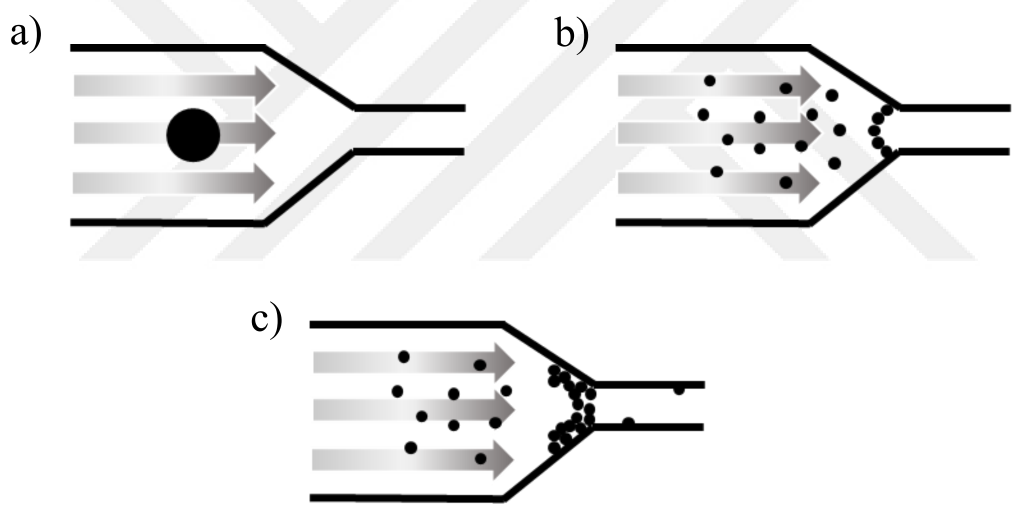

Figure 2 Illustration of clogging mechanisms: sieving (a), bridging (b), agglomeration (c).

Jamming may occur in dense suspensions with a bulk volume fraction between 0.2 and 0.6, where the local particle concentration reaches to jamming volume fraction (Dressaire & Sauret, 2017). However, it is not a requirement that the local concentration must be higher than the jamming value. The simultaneous arrival of particles to the constriction may be enough to form arches that can block flow (Dressaire & Sauret, 2017). It is possible to observe clogging due to bridge formation with a smaller number of particles if the flow velocity is above a threshold value. It has been reported that the increase in particle concentration, flow rate and the ratio of particle size to constriction width raises the probability of bridge formation (Marin et al., 2018). The other factors affecting the probability of arch formation are the lubrication flow and interparticle forces (Dressaire & Sauret, 2017).

The discussed clogging parameters above, the suspension particle loading, constriction geometry and flow rate are valid for particles with unsticking and smooth surfaces. However, when the surface becomes rough, the volume fraction required for jamming decreases in suspensions (Hsu et al., 2018) and increases the probability of jamming in dry systems (To et al., 2001). It is also worth mentioning that particle-particle surface interaction affects the probability of formation bridge (Dressaire & Sauret, 2017).

Particle roughness can be a crucial factor to consider for the explanation of clogging events in various technological applications (Brans et al., 2006; Pang et al., 2015; Vermes et al., 1987; Tavakkoli et al., 2015; Fuller et al. 2002). In this thesis, the impact of particle surface roughness on clogging events in a particle suspension flow through a constriction of a microfluidic channel. For this purpose, particles with five different roughness levels, with approximately 2 µm diameter, were produced and characterized to determine the effects of size and roughness. Next, particles were flowing was recorded in a microfluidic channel with a constriction by applying pressure. Finally, the image sequences obtained during the flow were analyzed to quantify particle volume fraction and flow velocity.

2) Experimental

a) Particle synthesis

The synthesis of raspberry-like silica particles with different roughness started with the smooth 1.98 µm silica particles (core particles) (Micro Particles, 5 % w/v, Germany). The smooth particles were cleaned to remove any possible organic compounds on the particle surface and activate the surface hydroxy groups. The cleaning was done by mixing aqueous smooth particle suspension with pre-heated ammonium hydroxide (NH_4OH) (SigmaAldrich, 28 % in water, Switzerland) and hydrogen peroxide (H_2O_2) (Merck Millipore, 30 %, Switzerland). An equal volume (4 ml) of ammonium hydroxide and hydrogen peroxide solution were poured in a round flask. The round flask was placed on a magnetic stirrer (Heidolph MR 2002, Germany) with an oil bath and heated up to 70 ℃. After the observation of bubble formation in the mixture, 4 ml (200 mg) of smooth particle suspension was added and mixed for 10 minutes. The obtained colloidal suspension was precipitated three times by centrifuging at 2500 rpm for 3 minutes (Hettich Rotofix 32, Germany). During each precipitation process, the supernatant was removed and the precipitate was dissolved in MilliQ (Merck Millipore). MilliQ was used instead of MilliQ water for all the following. In the end, the particle sediment was dispersed in 20 ml MilliQ.

To electrostatically adsorb smaller size silica particles (berry particles) on top of the core particles, their surfaces needs to have an opposite charge. For this purpose, the surface charge of core particles was reversed from negative to positive by adsorbing a polyelectrolyte 20 ml of cleaned core particle solution was mixed and stirred with 180 ml of Poly-DADMAC (0,025 wt %) at 500 rpm for 1 hour. The same precipitation procedure was followed like the previous step, to get rid of excess polyelectrolyte. In the end, the particle precipitate was re-dispersed in 40 ml MilliQ.

In this step, positively charged core particles and negatively charged berry particles were mixed to attach each other electrostatically. To do that, 10 ml (50 mg) of core particle suspension and 3 ml (1 wt %) of berry suspensions were mixed in a round flask on a magnetic stirrer at 500 rpm for 1 hour. In total, four raspberry-like particles with different roughness were prepared with 50 nm (NanoXact Silica Nanospheres, 10 mg/ml, USA), 75 nm (Nanocym, 10mg/ml, USA), 100 nm (NanoXact Silica Nanospheres, 10 mg/ml, USA) and 200 nm (NanoXact Silica Nanospheres, 10 mg/ml, USA) as berry particles together with the 1.98 µm core particles. The precipitation protocol, as above, was followed to get rid of unattached berry particles in the suspension. The precipitate was redispersed in 5 ml MilliQ in the end.

b) Particle smoothening

To be able to withstand shear in the flow experiment, the electrostatically adsorbed berry and core particles required to be permanently attached. For this purpose, a silica layer was grown on the particle with the means of a modified Stöber process (Graf et al., 2003; Zanini et al., 2017b). In a 100 ml Erlenmeyer flask, 5 ml of electrostatically stabilized raspberry-like particle solution, 6.2 ml NH_4OH, 38 ml ethanol (EtOH) (Sigma-Aldrich, Switzerland) were left to mix on a magnetic stirrer at 500 rpm. On the other side, tetraethyl orthosilicate (TEOS) (Sigma-Aldrich, 99.9 % in water, Switzerland) stock solution was diluted to 10 ml of 5 % solution with EtOH in a syringe. The syringe was placed on the flow rate control single syringe pump (New Era NE-1000 Programmable Single Syringe Pump, USA) and connected to the Erlenmeyer flask with a tube (Tygon 2001, Cole-Parmer). In total, 1.06 ml of 5% TEOS in EtOH solution was injected into suspension to smooth 50 mg of rough particles in four injection cycles. The last three smoothing cycles were carried out with sonication to avoid cluster formation and water cooling was applied to control the reaction temperature. However, the first cycle was done on a magnetic stirrer to prevent detachment of berry particles from the core particles. In each injection cycle, the TEOS solution was injected with a rate of 2 ml/hr in 8 minutes of injection time and 22 minutes of pause steps. The particle solution was centrifuged at 2500 rpm for 3 minutes immediately after completion of the last smoothening cycle to avoid further reaction which may cause particles to stick to each other. Next, the supernatant was replaced with MilliQ water and sonicated for 10 minutes. The sedimentation redispersion procedure was repeated three times to purify the raspberry-like particles.

The same smoothening procedure was applied to all raspberry-like particles with different berry size combinations.

c) SEM

Scanning electron microscope (SEM) is a type of electron microscope that images samples with a focused electron beam to produces images (Raghavendra & Pullaiah, 2018). In this project, it was used to measure the particle size, qualitatively analyze the shape and surface coverage of berry particles on the core particles. The average particle size calculation was done with ImageJ and at least 20 particles were measured from several different images. For the sample preparation, a piece of a silicon wafer was cleaned with ethanol and treated with UV/ozone before spreading 5 µL of particle suspension on it. In order to avoid surface charging, samples were sputter-coated (CUU-010, Safematic, Germany) with 3nm of Pt before SEM imaging.

d) AFM

Atomic force microscopy (AFM) is an advanced scanning probe microscopy technique (Singer et al., 2019). It has three main functions: topographic imaging, force measurement and manipulation. In this project, AFM (NanoWizard NanoOptics, JPK Instruments AG, Germany) was used because of its capabilities on obtaining surface roughness information. The AFM samples were prepared by dropping 5 µL particle suspension and spreading on a UV/ozone-cleaned round glass slides.

Three types of rough particles with 50 nm, 75 nm and 100 nm berries, minimum 16 particles of each kind, were imaged in tapping mode. The surface topography of particles with 75 nm berries were recorded with 6 µm/s tip velocity in 6×6 μm^2 scanning area with 512 × 512-pixel resolution which covers multiple particles. On the other hand, particles with 100 nm berries were recorded with 2.5 µm/s tip velocity in 2.5 × 2.5 μm^2 scanning area with 128 × 128-pixel resolution which covers single particle to avoid particle dragging. The particles with 50 nm berries were analyzed both as a group and individually to ensure the scanning method does not have an impact on the surface roughness result. The other relevant recording parameters were 0.5 Hz line rate, 1.0 s half scan time and 10 % overscan.

Root-mean-square roughness (RMS roughness) was used to describe and compare the roughness of the particles with a single parameter. It was extracted in four steps from the obtained topographical data by a Mathematica custom-made code. In the first step, band-pass filters were applied to the images and particle centers were assigned to the local maxima of the images. Second, the radius was fitted by using the measured SEM values. Third, the fitted radius was used to construct a volume of the particles. The volume was decoupled from the curvature originated from the shape of the particle to obtain the true surface topography on an artificially flattened surface. The surface was limited to the largest possible square frame inscribed on it. In the final step, the RMS roughness is calculated by taking mean square average of the oscillations perpendicular to the surface.

e) Microfluidic channel production

The microfluidic chips used in the flow tests consist of two main parts, polydimethylsiloxane (PDMS) and a glass slide. The PDMS part holds the dumbbell shape like quasi-2D microfluidic channel design (Figure 3) and these channels were enclosed with glass slides. The two circular ends of the designs were used for attaching an inlet and outlet tubes. The two sets of pillar grids were placed to filter impurities and particle clusters by sieving. The channel was designed to observe behavior in converging flow. For this reason, the width of the middle section gets narrower with two 45° angle steps. The initial channel with 500 μm width scales down to 24 μm in the first step. In the narrowest part of the channel, the 24 μm channel scales down to 6 μm and forms a square cross-section. The ratio of 6 μm channel width D to approximately 2 μm particle diameter d provide D/d = 3. It was observed by Marin et al. that, clogging is possible to occur when D/d ≈ 3 (Marin et al., 2018), even with dilute suspensions. On the other hand, the flow becomes uninterrupted even for intense volume fraction increases at D/d > 3.

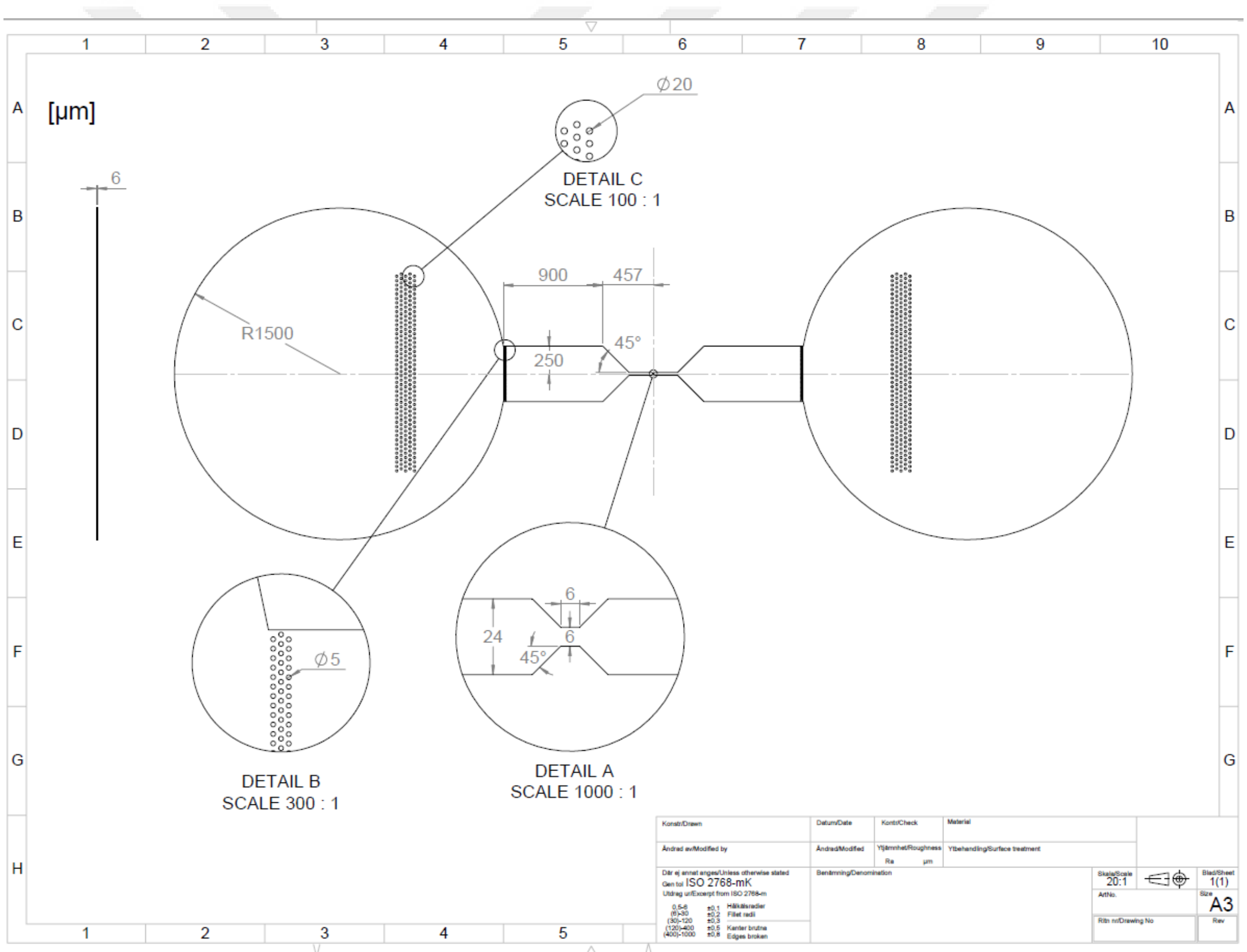

Figure 3 Drawing of the microfluidic channel design.

Channels were fabricated from PDMS (SYLGARD 184, USA), which is a widely used silicon-based organic polymer for microdevice fabrication. In the beginning, the two component of the PDMS kit were poured in a container by following a 10:1 polymer/curing agent ratio. This mixture was mixed with 2000 rpm for 1 minute and degassed for 1 minute with the help of mixing and degassing machine (THINKY ARE-250, UK). The thoroughly mixed and degassed mixture was poured carefully on a master with multiple channels, which was produced by Mycronic AB and left to cure for 24 hours at 70 °C. Afterward, the cured PDMS was gently removed from the master and two holes were punctured at the end of each channel to introduce inlet and outlet holes. Each microfluidic channel was carefully separated from the other channels individually and robustly rinsed with ethanol.

In the final step, the PDMS part and glass slide were bonded to each other to seal the channels. This was done by treating surfaces of PDMS and glass slide for 2 minutes by Oxygen plasma cleaner (Plasma Cleaner/Sterilizer PDC – 32 G). Prior to the plasma treatment, the glass slide was sonicated and rinsed with toluene, isopropanol, EtOH, MilliQ and dried with pressurized nitrogen to get rid of contaminations.

f) Flow experiments

The flow experiments were performed by using the setup in Figure 4. The microfluidic chip (Figure 4 a) was mounted on the stage of the inverted microscope (Zeiss Axio Obsever, Germany). The image acquisition was done with 63 X objective (Figure 4 b) (Zeiss, Germany) combined with a camera (Zyla 5.5 sCMOS) mounted on the microscope.

The sample and MilliQ reservoirs (Figure 4 c and d) (15 mL Falcon Tube, Elve Flow, France) were connected to a pressure control pump (Figure 4 e) (MK3, ElveFlow, France) at one end and connected to the channel inlet at the other end via Teflon tubing (PTFE Teflon Tubing, 1/16 inch outer diam., 1/32 inch inner diam., ElveFlow, France). An air pressure source (Figure 4 f) fed the pump to provide pressure in the setup. Both pressure software (Elveflow MK3 – ESI

Microfluidic Software) and image acquisition software (Micro-Manager Version 2.0-gamma) were monitored and controlled via a computer (Figure 4 g).

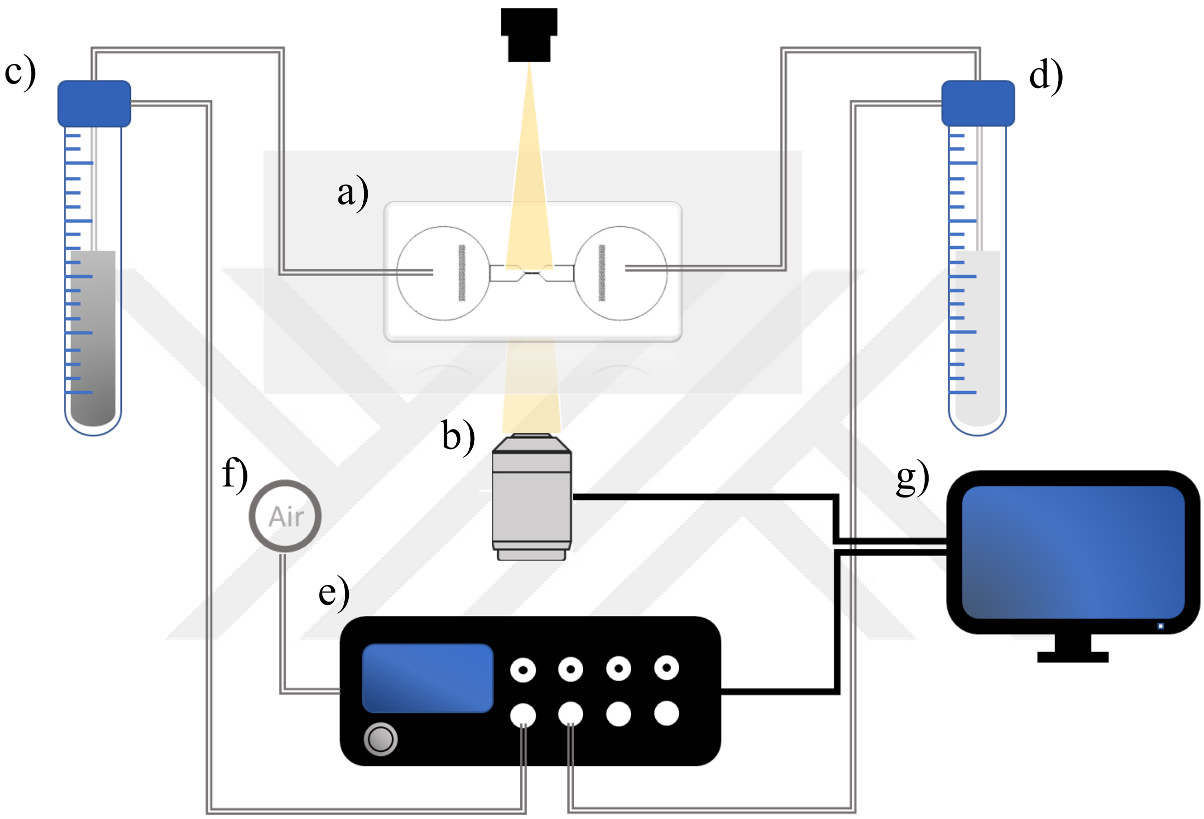

Figure 4 Illustration of the flow experiment setup which includes microfluidic chip (a), camera objective and camera (b), particle suspension (c) and (d) water reservoirs, pressure pump (e), pressure source (f) and control computer (g).

In the beginning, the pressure of the MilliQ and sample reservoirs were set to 10 mbar. Before connecting the sample reservoir tube to the test system, the channel was flushed and filled with MilliQ to remove contaminations in the channels, test the sealing of the channels and ease the inflow of the particle solution. For this purpose, the MilliQ reservoir was connected to the channel, the pressure was increased from 10 mbar to 200 mbar with 1 mbar/sec rate and waited until observing a water droplet at the other inlet of the channel.

In the next step, the sample reservoir with 0.1 wt% aqueous particle suspension was connected to the available channel inlet and the pressure was increased from 10 mbar to 200 mbar like the MilliQ reservoir. Both reservoir's pressure was held at 200 mbar until removing all air bubbles in the channel and both pressures were decreased to 20 mbar steadily with a rate of 1 mbar/sec. The sample reservoir pressure was then increased gently until observing mild particle flow in the channel. In order to increase the concentration of the particles in the region of interest, the glass slide inclined toward the water reservoir direction (Figure 5) with a chock and waited from an hour to overnight depends on the particle suspension and flow speed.

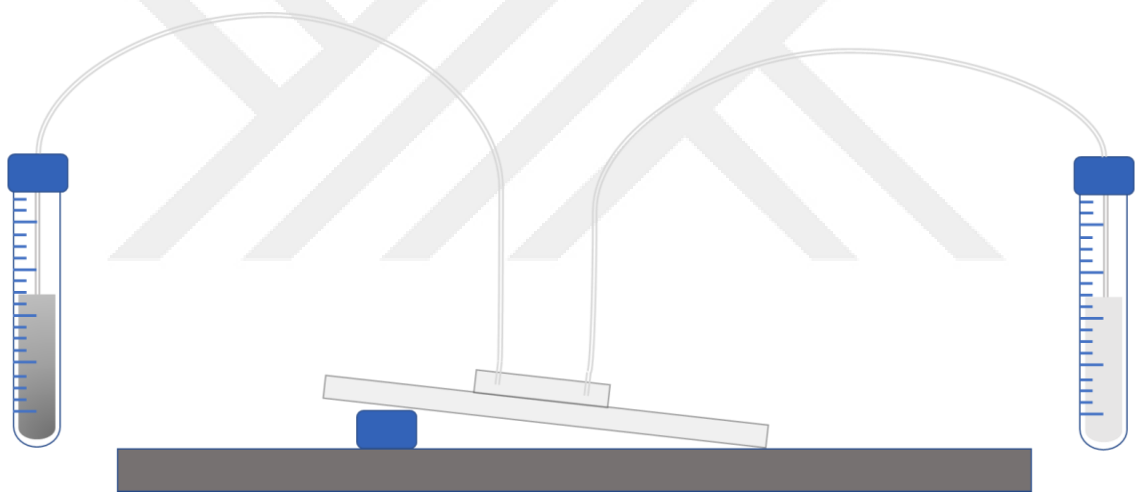

Figure 5 Illustration of the tilted setup to increase particle concentration in the channel.

After particles were sedimented around the constriction region, the chock was removed and the glass slide was stabilized on the microscope stage. The flow inside the channel was gradually reversed by increasing pressure from the MilliQ reservoir side until finding optimum pressure where the particles stayed stationary. After that point, two different flow protocols were followed depending on the clogging behavior of the particles. The first flow protocol was used for particles that can unclog the constriction easily by reversing the flow. In this protocol, image acquisition was done by particles flowing through the constriction back and forward with 30 seconds of periods while clogging and unclogging. The second flow protocol was used for particles that tend to stay in the constriction region when the flow was reversed. In this protocol, the flow was applied continuously in one direction and the channel was tapped gently to unclog after each clogging event.

To obtain data set with a wide velocity range, the pressure difference between the two reservoirs varied between 0.2 and 5 millibars. However, the pressure difference may not be correlated with the particle velocity in the channel. Because the particle concentration in the tubes and both ends of the channel effects how the applied pressure converted to the pressure difference in the constriction. For this reason, image analysis was done to extract the velocity values.

g) Image acquisition and analysis

i) Image acquisition

Image sequences were acquired from a region of interest (ROI) including the constriction and an adjacent area, which allows to track particles. Dimensions of the chosen rectangular ROI (Figure 6 a) was 1600 pixels in length (l_{ROI}) and 250 pixels in height (h_{ROI}). The region corresponds to 165 × 32.5 μm^2 with resolution of 0.103 μm/pixel.

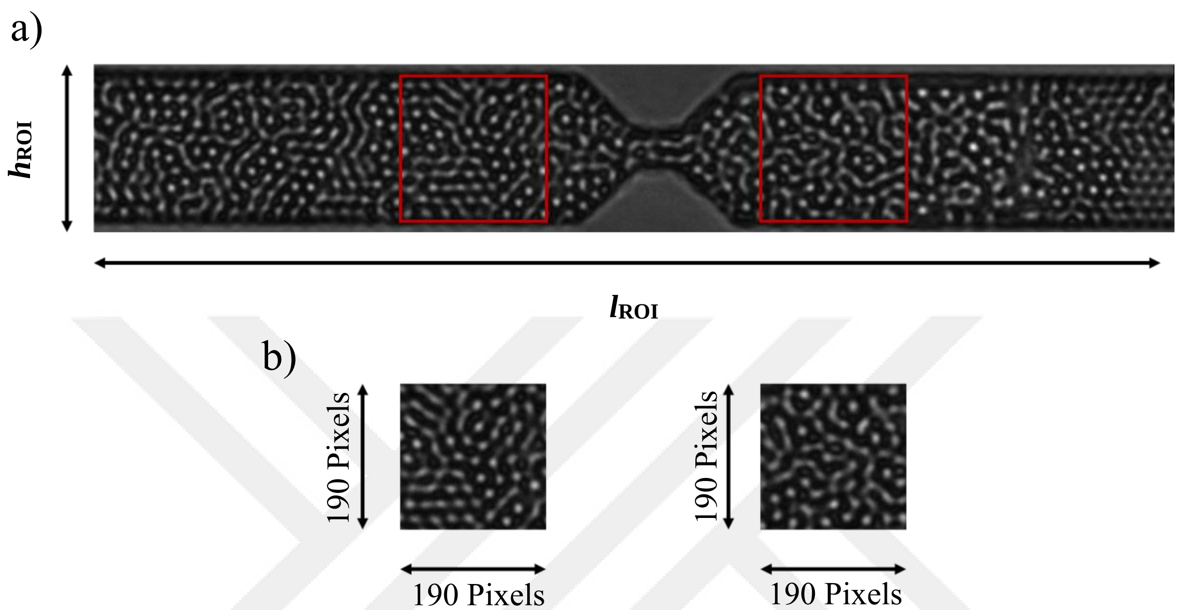

Figure 6 Illustration of the acquired ROI (a) and cropped ROI for image processing (b).

Images were acquired in every 0.05 seconds, which corresponds to 20 frames per second. Each data sets obtained with the second flow protocol, mentioned in the previous section, were cropped into smaller data sets containing an individual clogging event, which consists of 40 to 320 frames (Appendix 1 and 3). On the other hand, data sets from the first flow protocol were acquired and analyzed in uncropped forms. With this protocol, 6000 images were acquired continuously over 5 minutes (Appendix 2).

ii) Preparation for image analysis

The acquired images were converted to 8-bit images from 16-bit images and cropped into two smaller regions of interest to perform quantitative and qualitative image analysis.

Image analysis was performed in the upstream of the constriction to quantify volume fraction and average velocity in the flow direction. Image stacks were manually cropped into two 190 × 190 pixels square frames (Figure 6 b) which corresponds to 19.6 × 19.6 μm^2, considering the flow in both directions.

Spatiotemporal diagrams were automatically generated by a MATLAB code.

iii) Spatiotemporal diagrams

It is not practically possible to present the large collected amount of microscopy images individually. Spatiotemporal diagrams were prepared for each clogging event or full data set, depending on the followed flow protocol, to visualize and qualitatively analyze the clogging events.

Spatiotemporal data analysis is used to analyze a phenomenon in a singular location and a specified period. In this study, a rectangular band, which is one pixel thick and wide as the length of the ROI image through the constriction, was selected as the location (exaggerated frame in Figure 7 a). The period was set by the image acquisition time. For this reason, the image bands were collected from each image of stacks during the whole image acquisition. In the next step, these thin image bands from each image are stacked on top of each other through the y-axis to form the diagram (Figure 7 b). The x-axis of the figure is correlated with space and the y-axis is correlated with time. The clogging events are marked on the Figure 7 b.

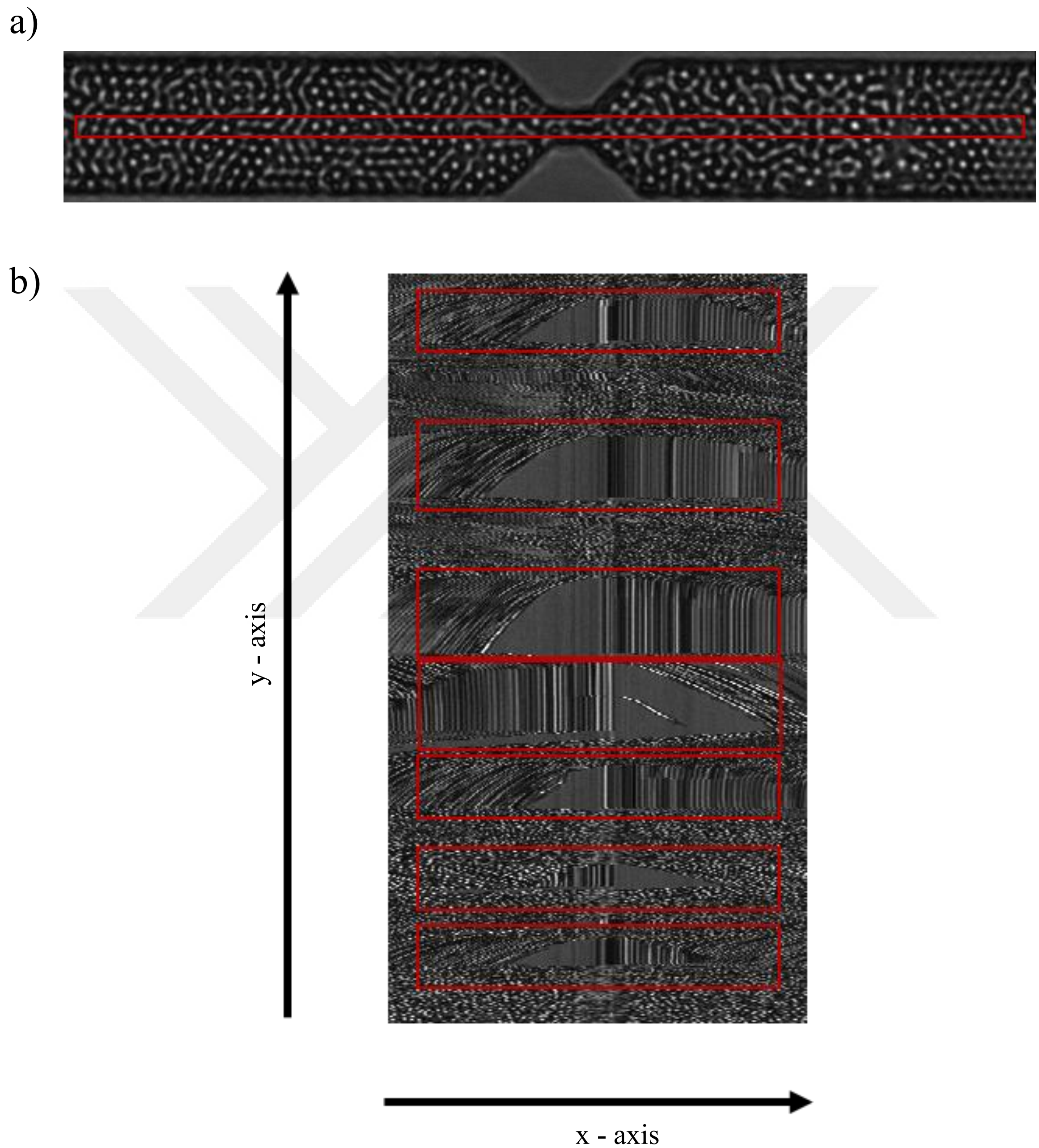

Figure 7 Illustration of the exaggerated band-like frame (a) and spatiotemporal diagram which shows 7 marked clogging events (b).

iv) PIV

PIV (Particle Image Velocimetry) is an optical method to visualize flow and thus collect velocity and related fluid characteristics. The fundamental idea is detecting motion by correlating different parts of images in the presence of tracers. Alternatively, whenever possible to track individual particles, the coordinates of particle centers ban be used to construct the trajectories of the particles (Isa, 2008).

In the traditional setup for PIV, a thin sheet of laser light is projected into a fluid consisting of reflective and buoyant tracer particles (Thielicke & Stamhuis, 2014). A CCD camera located parallel to the sheet of laser light, records subsequent images at t_0 and $t_0+\Delta t$. Particles were tagged in a frame and tried to tag the same particles in the subsequent frame. The velocity was calculated from particle displacement between two frames and the Δt.

In this project, PIV was used to obtain velocity from cropped image stacks of the upstream of constriction (see the chapter preparation for image analysis). The contrast between particle and the background was used instead of illuminating laser on reflective particles.

The Matlab PIVlab - particle image velocimetry (PIV) tool (Thielicke, 2020) was used to analyze, validate and visualize the flow. Cross-correlation of many small sub-images (interrogation areas) was evaluated to extract particle displacement for groups of particles. Images were imported with 1-2,2-3,3-4 sequencing style. In the pre-processing step, contrast limited adaptive histogram equalization (CLAHE) with 20-pixel window size and auto contrast stretching were applied. For the PIV settings, FFT window deformation was used as the algorithm and Interrogation areas were set to 32 and 16 for pass 1 and pass 2, respectively. Time step and reference distance calibration were done before the analysis. After the analysis, vector validation was completed manually by eliminating from velocity scatter plot to get rid of vectors on the opposite and perpendicular to the flow direction (Figure 8). In the last step, the frame before the clogging was chosen and the area mean flow direction velocity was extracted.

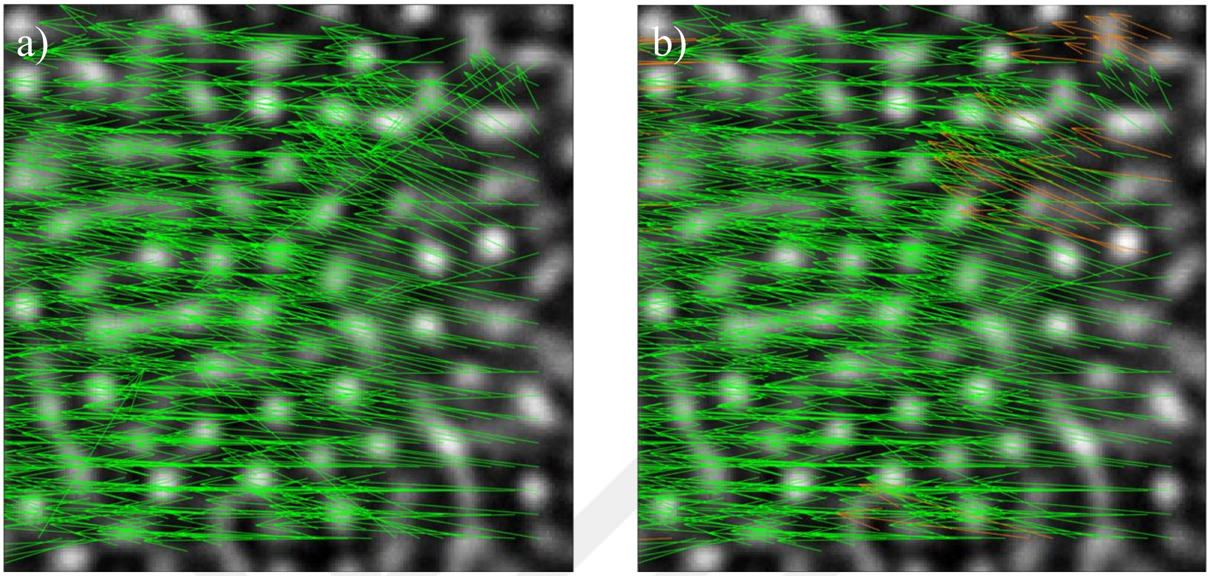

Figure 8 Illustration of the PIV results before (a) and after (b) vector validation.

v) Particle tracking

Particle tracking was performed to locate the particles in the frame and extrapolating it to the volume fraction. A custom-made Matlab code scripted initially by Maria Kilfoil was used to analyze both upstream and downstream of the constriction (see the chapter preparation for image analysis). Particle size, minimum integrated intensity, maximum allowed squared radius of gyration and eccentricity were introduced to the code as an input. The parameters changed between each data set because of the particle size change due to the berries, focus, channel thickness, room lighting. Before analyzing the data set, the parameters were tested on frames with a dense and a dilute flow to optimize the particle detection performance (Figure 9). The green circles represent the accepted particles and red dots are rejected particles.

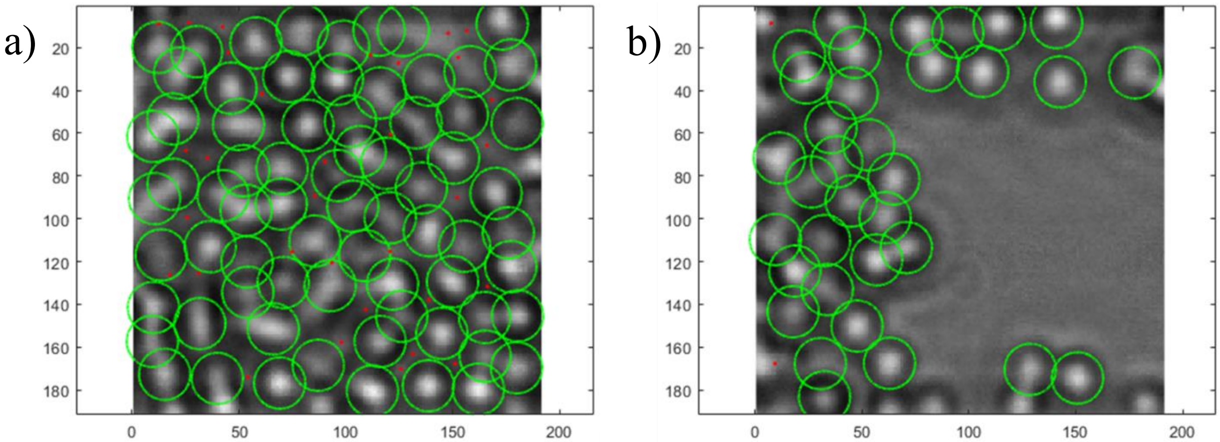

Figure 9 Illustration of detected particles with optimized parameter for dense (a) and dilute (b) frame.

In order to calculate the volume fraction (ϕ), the number of particles in the frame ($N_{particles}$) multiplied by the volume of a single particle ($V_{single\ particle}$) divided by corresponding frame volume (V_{frame}) as in Equation 1.

$$\phi = \frac{N_{\text{particles}} \times V_{\text{single particle}}}{V_{\text{frame}}} \qquad (1)$$

The volume fraction was used instead of area fraction due to the limitation of the detection system. The setup was not able to resolve particle coordinate in 3D which prevent to interpret on particles monolayer formation (Figure 10 b) or even distribution (Figure 10 c) in the volume. Therefore, the number of counted particles from the top of the volume (Figure 10 a) are extrapolated to 3D.

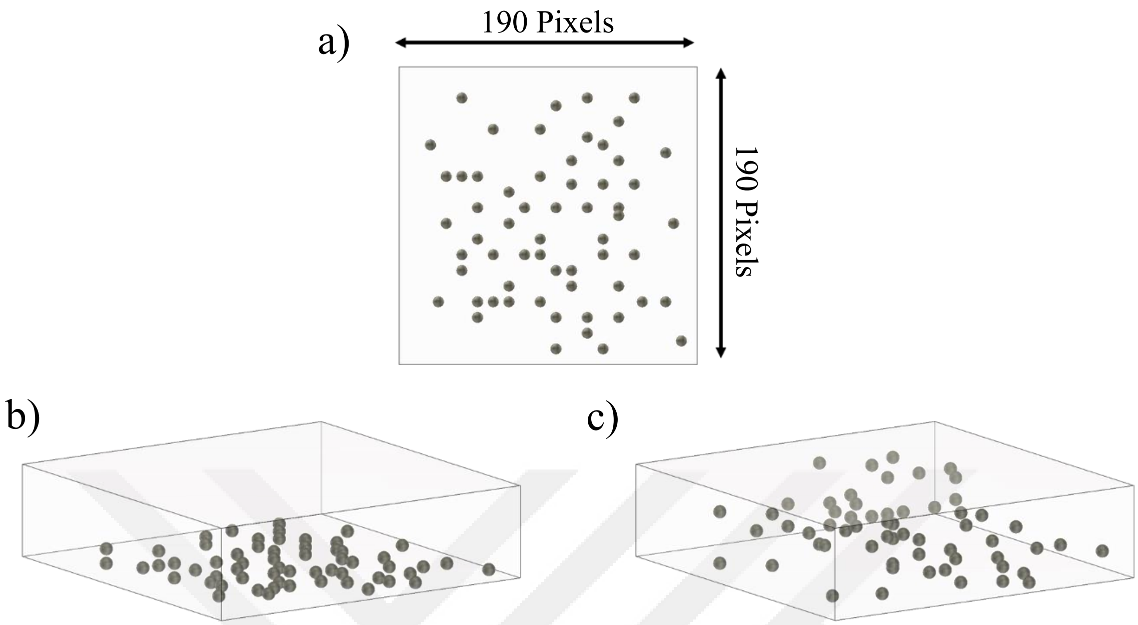

Figure 10 Illustration of an imaginary frame recorded from top (a) and two particle configuration possibilities in 3D: monolayer formation (b) and even distribution (c).

All the particles with different berries assumed to be spheres in this calculation. The particle volumes were calculated based on their diameter measurement in SEM images. For the calculation of the frame volume, 6 μm channel height and the frames size 19.6 × 19.6 μm^2 were used.

3) Results

a) SEM

The SEM images of five particles are presented in Figure 11. The measured average particle size and its standard deviation for three different raspberry-like particles are shown in Table 1.

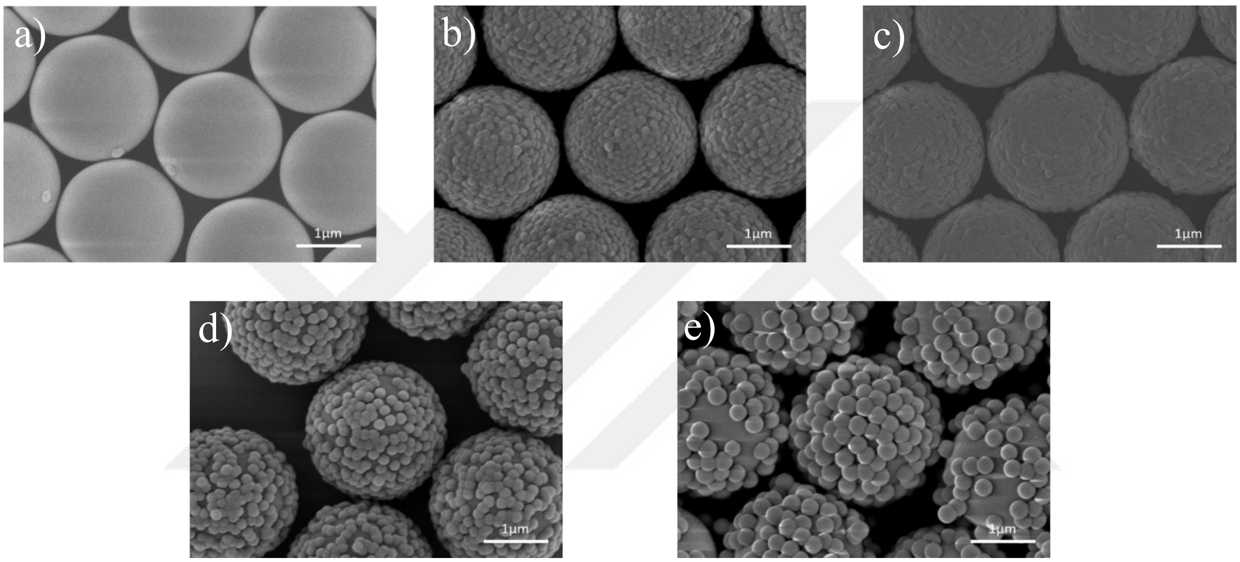

Figure 11 SEM images of smooth particles (a) and raspberry-like particles with 50 nm (b), 75 nm (c), 100 nm (d) and 200 nm (e) berry particles.

Table 1 Particle diameter and standard deviation of the measurement obtained from the SEM images

Berry Size (nm)	Average Diameter (nm)	Standard Deviation (nm)
50	2078	54
75	2183	53
100	2206	45

b) AFM

The AFM surface topography images of particles acquired with different measurement types are presented in Figure 12. The calculated average RMS roughness and its standard deviation for three different raspberry-like particles are shown in Table 2.

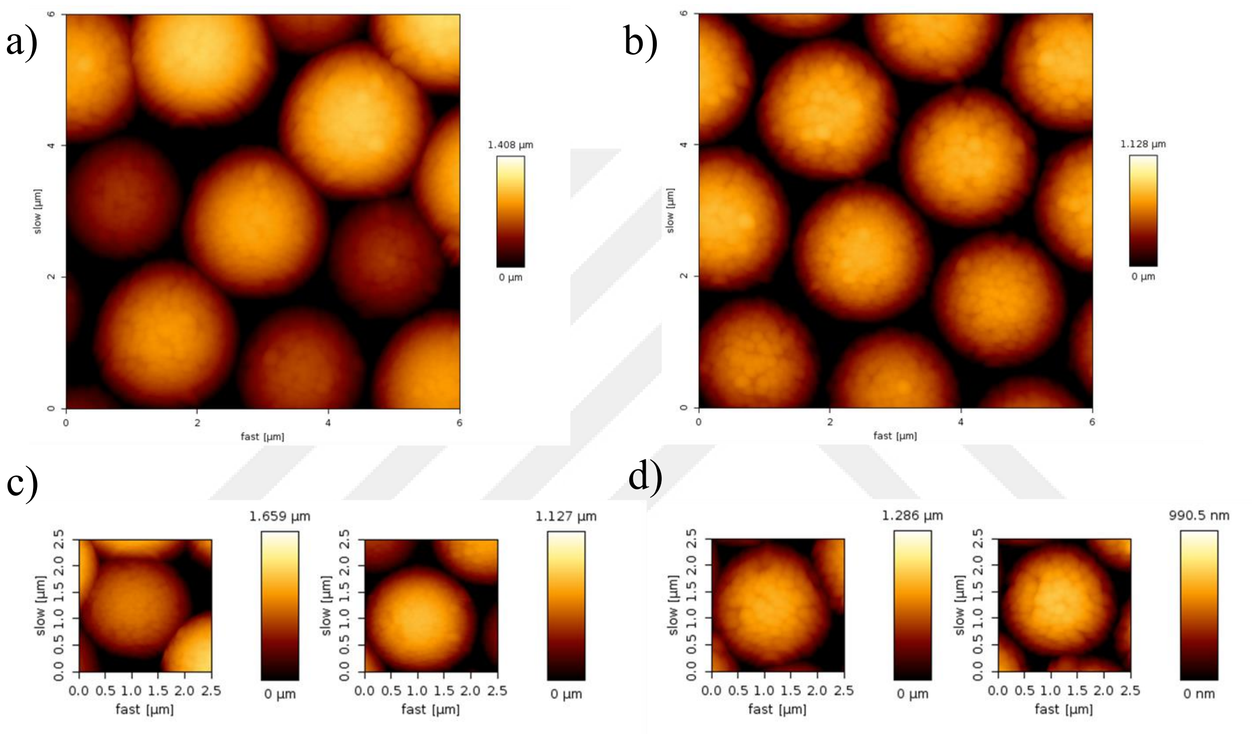

Figure 12 AFM surface topography images of raspberry-like particles with 50 nm (a) and 75 nm (b) berry particles obtained by scanning multiple particles and 50 nm (c) and 100 nm (d) berry particles obtained by scanning single particles.

Table 2 RMS roughness and its standard deviation extracted from obtained surface topography images of three different particles with two different measurement types.

Berry Size (nm)	Measurement type	Average RMS Roughness (nm)	Standard Deviation of RMS Roughness (nm)
50	Multiple Particles	9.8	1.7
50	Single Particle	10.3	2
75	Multiple Particles	14.3	2.1
100	Single Particle	20.7	6.1

c) Flow experiments

The synthesized raspberry-like particles were tested and analyzed to correlate particle surface roughness and the clogging characteristics. PIV was used to measure the particle velocity from the ROI. The number of particles was measured with particle tracking and extrapolated to volume fraction. Figure 13 presents the volume fraction and average velocity dependency of the clogging events for the particles with 50 nm, 75 nm and 100 nm berries. Each spot on the graph represents an individual clogging event. The relationship between the measured RMS particle surface roughness average and the average of the measured flow direction mean velocity was shown in Figure 14.

Tests with smooth particles were conducted and clogging events were observed at very high velocities, which are out of our detection limits. On the other hand, the particles with the 200 nm berries were introduced to the flow setup. However, after the pressure application, the particles tended to agglomerate and irreversibly clog the channels (Appendix 4).

The clogging event caused by particle agglomerates, impurities in the suspension or channel imperfections were eliminated before the analysis stage and they were not included in the presented data.

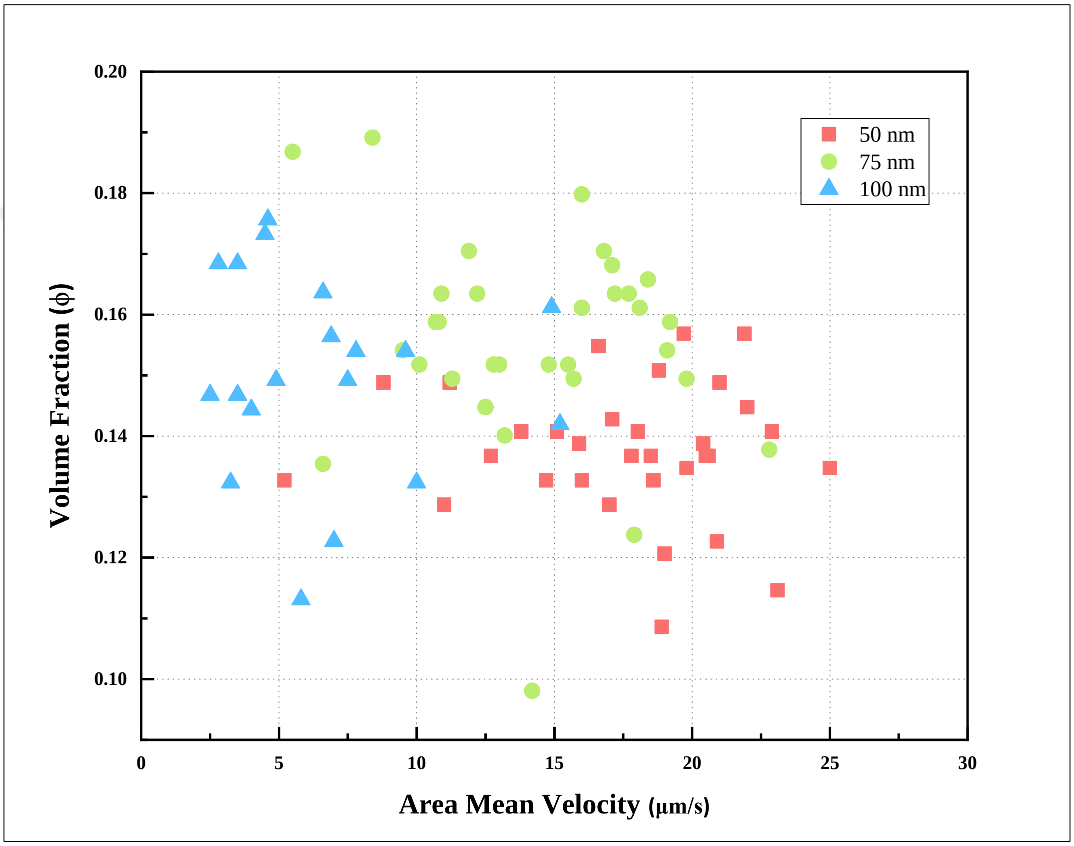

Figure 13 Clogging occurance respecting the particle volume fraction and area mean particle velocity in the flow direction for raspberry-like particles with 50 nm, 75 nm and 100 nm berry particles. Each point represent an individual clogging event.

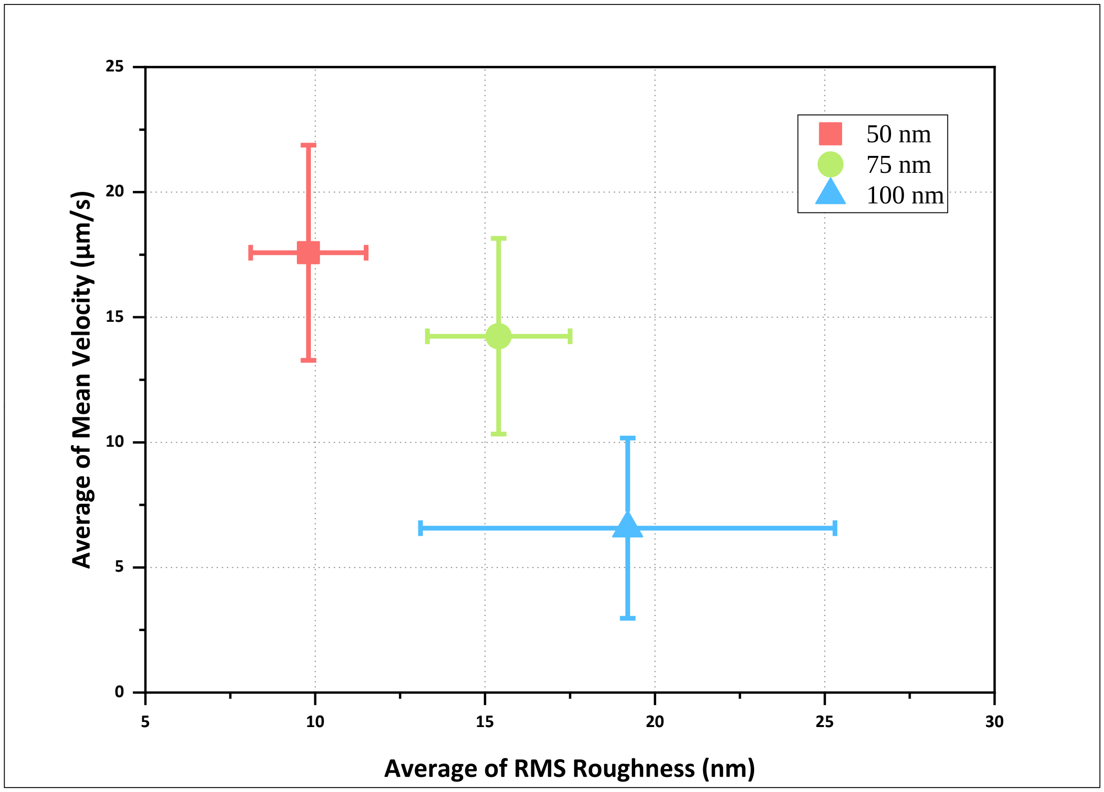

Figure 14 Clogging occurrence for particles with respect to the measured area mean particle velocity average and RMS roughness average.

4) Discussion and conclusion

Spatiotemporal diagrams give an idea about the nature of the clogging events. In the flow experiment at the constriction, clogs formed in the upstream part of the flow and stopped the motion of particles, as expected. The particles stopped in the constriction form vertical lines in the diagram. The height of the vertical lines gets shorter through the upstream direction due to the accumulation of particles at the upstream of the flow by the time. On the downstream side, clogging causes the flow speed to decrease and forms curved velocity lines in the side of the diagram. From these diagrams, it is hard to deduce the mechanism of the clog formation such as bridging or aggregation.

The SEM images were recorded for smooth and four raspberry-like particles with 50 nm, 75 nm, 100 nm and 200 nm berries. The particle size measurement showed that raspberry-like particle size increases with the increase in berry size, as expected. The surface coverage of the particles decreases with the increase in the berry size. As discussed by Zanini et al. (2017a), this may be due to the increase of the asperity size, which causes geometrical restriction and obstructs the new berry particle to attach in the region between berries during the particle synthesis.

The particle surface topography images were acquired with AFM. RMS roughness value was extracted for three different particles. Based on the RMS roughness values, the particles with bigger berries form a rougher surface. However, particles with higher RMS roughness value shows roughness results more scattered from the average RMS roughness. The increase in the RMS roughness standard deviation value for the raspberry-like particle with the 100 nm berry particle may stem from the heterogeneous surface coverage or particle drifting during the imaging.

In Figure 13, clogging events were pointed with respect to particle volume fraction and mean velocity for the raspberry-like particles with 50 nm, 75 nm and 100 nm berries. All clogging events were observed at a concentration below the jamming point of smooth particles. The clogging may have happened due to the jamming at lower concentrations due to the surface roughness (Hsu et al., 2018), or local processes such as bridging and aggregation (Dressaire &

Sauret, 2017). Although, it was not possible to decide on the dominant phenomena, increased particle interlocking due to asperities on the surface anyway causes clogging at lower concentrations compared to smooth particles.

A trend of decrease in the particle velocity and volume fraction was observed for the clogging of raspberry-like particles with bigger berry sizes and hence higher RMS roughness. Although, there is not a clear separation between the results of different particle types in Figure 13, clogging data for a wide range of volume fraction and velocities was recorded. Between $\phi = 0.13$ and $\phi = 0.16$, the required particle velocity to form a clog decreases with berry size. The difference between the clogging of the three particle types and the velocity trend is clearer in Figure 14, which presents the average of the measured mean velocities and average of RMS roughness data. The required average of the mean velocity for forming clog decreases with the particle surface roughness. In other words, the possibility of clogging formation is higher for particles with rougher surfaces.

In the region adjacent to the constriction, particle detection becomes harder and requires high image acquisition rates. The ROI on the channel was selected close to the constriction and the proximity was limited with particle detection limits. However, measuring particle volume fraction and velocity from a ROI distant from the constriction makes it difficult to comment on the effect of the local particle concentration of the clogging events.

The maximum velocity measured with the PIV was 25 μm/s and the particle volume fraction was ϕ=0.19. For the smooth particles, the velocity of the particles where the clogging occurred was out of the detection limit at the set camera fps and the PIV program was not able to track particles.

It has been observed during the flow experiments that the particles tend to form aggregates in the channel by the application of the pressure. This behavior becomes more pronounced for the particles with bigger berries. For this reason, the results of tested roughest particles with 200 nm berries could not be plotted in Figure 13 and 14. When the aggregates could be removed from the constriction easily by reversing flow, the channel was tapped gently to remove aggregates from the constriction. To remove the effect of tapping from the image sequences, they were divided into smaller image sequences each contains individual clog except the particles with 75 nm berries. The reason behind the agglomeration can be the hydrodynamic interactions between the rough particles under flow.

The effect of the used methodology for the particle tracking should be considered. For the volume fraction determination, the particle tracking method was used. The parameter selection for each data set was done manually and confirmed by testing on two different frames. Although the image sequences were kept small, it cannot be guaranteed to at all particles are detected in all the frames of the image sequence. In addition to that, the number of particles detected on 2D was extrapolated to 3D which does not provide an accurate number of particles in the channel.

The frame selection for defining the clogging event was done manually, which may introduce inconsistency to the test results. After the analysis of image sequences with PIV, the clogging frames were selected as the ones for which there is a discernible decrease relative to the average velocity in the subsequent frame. The selection was also filtered depending on the quality of the particle tracking for that frame.

The control over the parameters of the flow experiments was limited. The control parameter during the flow experiments was the pressure difference between the two reservoirs and the concentration of the solution in the reservoir. However, controlling these two parameters does not allow to precisely adjust the volume fraction of particles in the channel and flow speed of the particles. The logic was to manipulate the two parameters relatively and measure the changes in the flow speed and particle volume fraction.

To conclude, particles with rougher surfaces form clogs at lower particle velocity in a microfluidic channel with a constriction. The clogging formation behavior difference between the particles are obvious at $\phi \approx 0.15$.
The particles with higher surface roughness tend to form agglomerates with the application of pressure in microfluidic channel.

5) Outlook

The obtained results are consistent with the initial idea of the project. Surface roughness of the particles has an impact on the clogging behavior of colloidal particle flow in a microfluidic system. However, there is possibility of improvements for different steps of the study.

Higher image acquisition rate can be used. Image sequence recording with the higher fps may help to characterize the smooth particles in the test setup, besides the particle concentration increase up to the jamming concentration. Moreover, higher acquisition rate may allow to move the ROI frames adjacent to the constriction to collect information about the local processes and concentrations.

The effect of channel geometry on the clogging characteristics of particles was studied. In this thesis the critical ratio studied in Marin et al. (2018) for smooth particles was used. The effect of surface roughness on the critical ratio can be analyzed. Different constriction width to particle diameter ratios, approaching angle to the constriction and particle sizes can be tested to investigate the effect of the geometry.

Particle volume fraction measurement can be improved by introducing fluorescence in to the particles. Detecting fluorescent particles in a fluorescent microscope leads to an increase of contrast between particle and the background. This would help particle tracking program to identify particles. In addition to that, fluorescent particles in a confocal fulorescence microscope provide 3D resolution of particles and give more accurate result compare to the extrapolation of 2D number of particles.

The study can be extended by introducing new parameters. The study of Hsu et al. (2018) showed that particle polydispersity in terms of roughness increase the jamming transition concentration. Particles with different roughness's can be combined and compared with monodisperse systems to observe its effect on the clogging behavior. In addition to that, tests can be conducted with soft particles and carrying fluids with various viscosities.

6) References

Bacchin, P., Marty, A., Duru, P., Meireles, M., & Aimar, P. (2011). Colloidal surface interactions and membrane fouling: Investigations at pore scale. *Advances in Colloid and Interface Science*, *164*(1–2), 2–11. https://doi.org/10.1016/j.cis.2010.10.005

Brans, G., Kromkamp, J., Pek, N., Gielen, J., Heck, J., van Rijn, C. J. M., Boom, R. M. (2006). Evaluation of microsieve membrane design. *Journal of Membrane Science*, *278*(1–2), 344–348. https://doi.org/10.1016/j.memsci.2005.11.018

Campbell, A. I., & Haw, M. D. (2010). Jamming and unjamming of concentrated colloidal dispersions in channel flows. *Soft Matter*, *6*(19), 4688–4693. https://doi.org/10.1039/c0sm00110d

Donev, A., Cisse, I., Sachs, D., Variano, E. A., Stillinger, F. H., Connelly, R., Chaikin, P. M. (2004). Improving the density of jammed disordered packings using ellipsoids. *Science*, *303*(5660), 990–993. https://doi.org/10.1126/science.1093010

Dressaire, E., & Sauret, A. (2017). Clogging of microfluidic systems. *Soft Matter*, *13*(1), 37–48. https://doi.org/10.1039/C6SM01879C

Fernandez, N., Mani, R., Rinaldi, D., Kadau, D., Mosquet, M., Lombois-Burger, H., … Isa, L. (2013). Microscopic mechanism for shear thickening of non-brownian suspensions. *Physical Review Letters*, *111*(10), 1–5. https://doi.org/10.1103/PhysRevLett.111.108301

Fuller, S. B., Wilhelm, E. J., & Jacobson, J. M. (2002). Ink-jet printed nanoparticle microelectromechanical systems. *Journal of Microelectromechanical Systems*, *11*(1), 54–60. https://doi.org/10.1109/84.982863

Graf, C., Vossen, D. L. J., Imhof, A., & Van Blaaderen, A. (2003). A general method to coat colloidal particles with silica. *Langmuir*, *19*(17), 6693–6700. https://doi.org/10.1021/la0347859

Helbing, D., Farkas, I. & Vicsek, T. (2000). Simulating dynamical features of escape panic. *Nature*, *407*, 487–490. https://doi.org/10.1038/35035023

Hsu, C. P., Ramakrishna, S. N., Zanini, M., Spencer, N. D., & Isa, L. (2018). Roughness-dependent tribology effects on discontinuous shear thickening. *Proceedings of the National Academy of Sciences of the United States of America*, *115*(20), 5117–5122. https://doi.org/10.1073/pnas.1801066115

Isa, L. (2008). *Capillary flow of dense colloidal suspensions* (Doctoral thesis, The University of Edinburgh, Edinburgh, Scotland). Retrieved from http://hdl.handle.net/1842/2600

Kim, J., Erath, J., Rodriguez, A., & Yang, C. (2014). A high-efficiency microfluidic device for size-selective trapping and sorting. *Lab on a Chip*, *14*(14), 2480–2490. https://doi.org/10.1039/c4lc00219a

Marin, A., Lhuissier, H., Rossi, M., & Kähler, C. J. (2018). Clogging in constricted suspension flows. *Physical Review E*, *97*(2). https://doi.org/10.1103/PhysRevE.97.021102

Pang, L., Shen, S., Ma, C., Ma, T., Zhang, R., Tian, C., Wang, J. (2015). Deformability and size-based cancer cell separation using an integrated microfluidic device. *Analyst*, *140*(21), 7335–7346. https://doi.org/10.1039/c5an00799b

Pournin, L., Ramaioli, M., Folly, P., & Liebling, T. M. (2007). About the influence of friction and polydispersity on the jamming behavior of bead assemblies. *European Physical Journal E*, *23*(2), 229–235. https://doi.org/10.1140/epje/i2007-10176-5

Raghavendra, P., & Pullaiah, T. (2018). Biomedical imaging role in cellular and molecular diagnostics. *Advances in Cell and Molecular Diagnostics*, 85–111. https://doi.org/10.1016/b978-0-12-813679-9.00004-x

Singer, A., Barakat, Z., Mohapatra, S., & Mohapatra, S. S. (2019). Nanoscale drug-delivery systems. *Nanocarriers for Drug Delivery*, 395–419. https://doi.org/10.1016/b978-0-12-814033-8.00013-8

Tavakkoli, M., Grimes, M. R., Liu, X., Garcia, C. K., Correa, S. C., Cox, Q. J., & Vargas, F. M. (2015). Indirect method: A novel technique for experimental determination of asphaltene precipitation. *Energy and Fuels*, *29*(5), 2890–2900. https://doi.org/10.1021/ef502188u

Thielicke, W., & Stamhuis, E. J. (2014). PIVlab – Towards User-friendly, Affordable and Accurate Digital Particle Image Velocimetry in MATLAB. *Journal of Open Research Software*, *2*. https://doi.org/10.5334/jors.bl

To, K., Lai, P. Y., & Pak, H. K. (2001). Jamming of granular flow in a two-dimensional hopper. *Physical Review Letters*, *86*(1), 71–74. https://doi.org/10.1103/PhysRevLett.86.71

Vermes, I., Steinmetz, E. T., Zeyen, L. J. J. M., & van der Veen, E. A. (1987). Rheological properties of white blood cells are changed in diabetic patients with microvascular complications. *Diabetologia*, *30*(6), 434–436. https://doi.org/10.1007/BF00292548

William Thielicke (2020). PIVlab - particle image velocimetry (PIV) tool (https://www.mathworks.com/matlabcentral/fileexchange/27659-pivlab-particle-image-velocimetry-piv-tool), MATLAB Central File Exchange. Retrieved April 18, 2020.

Wu, X. L., Måløy, K. J., Hansen, A., Ammi, M., & Bideau, D. (1993). Why hour glasses tick. *Physical Review Letters*, *71*(9), 1363–1366. https://doi.org/10.1103/PhysRevLett.71.1363

Zanini, M., Hsu, C. P., Magrini, T., Marini, E., & Isa, L. (2017). Fabrication of rough colloids by heteroaggregation. *Colloids and Surfaces A: Physicochemical and Engineering Aspects*, *532*(February), 116–124. https://doi.org/10.1016/j.colsurfa.2017.05.084

Zanini, M., Marschelke, C., Anachkov, S. E., Marini, E., Synytska, A., & Isa, L. (2017). Universal emulsion stabilization from the arrested adsorption of rough particles at liquid-liquid interfaces. *Nature Communications*, *8*, 1–9. https://doi.org/10.1038/ncomms15701

Zuriguel, I., Parisi, D. R., Hidalgo, R. C., Lozano, C., Janda, A., Gago, P. A., … Garcimartín, A. (2014). Clogging transition of many-particle systems flowing through bottlenecks. *Scientific Reports*, *4*, 1–8. https://doi.org/10.1038/srep07324

7) Appendix

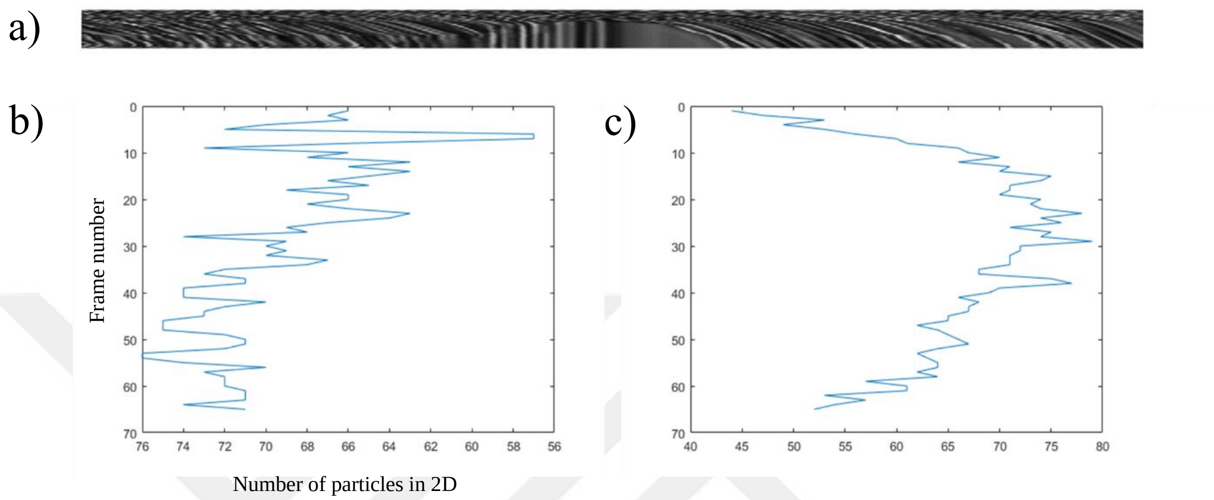

Appendix 1 Spatiotemporal diagram (a) and particle counting for left (b) and right (c) of the constriction. Individual clog formation by Raspberry-like particles with 50 nm in the microfluidic channel.

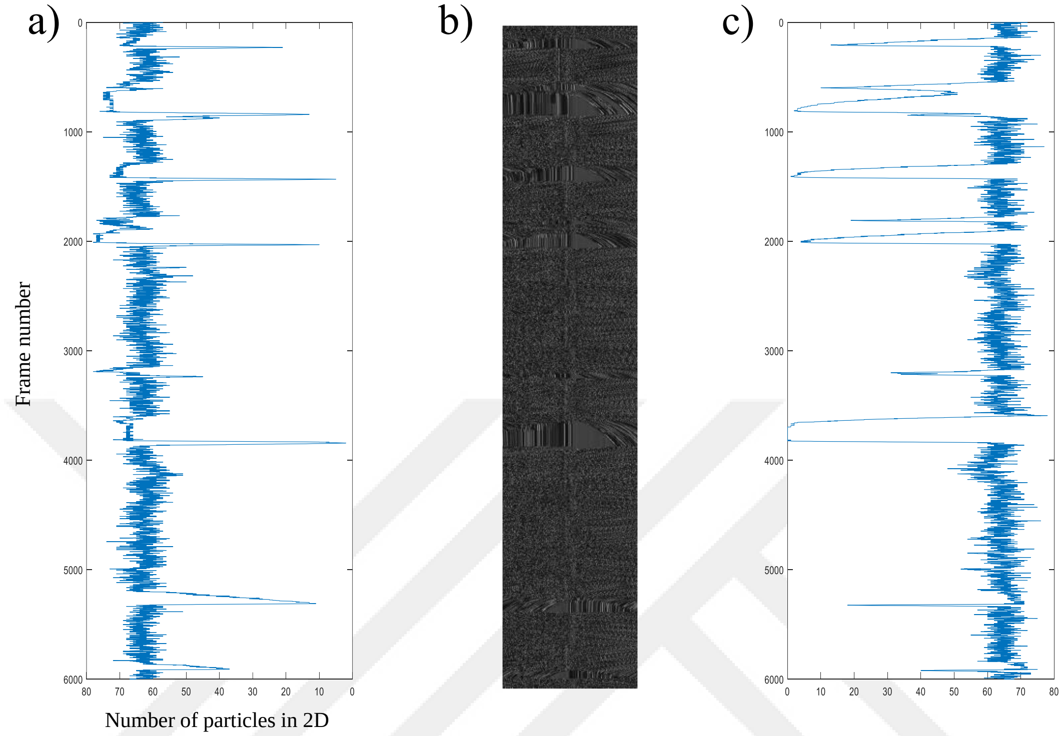

Appendix 2 Spatiotemporal diagram (b) and particle counting for left (a) and right (c) of the constriction. Multiple clog formation by Raspberry-like particles with 75 nm in the microfluidic channel.

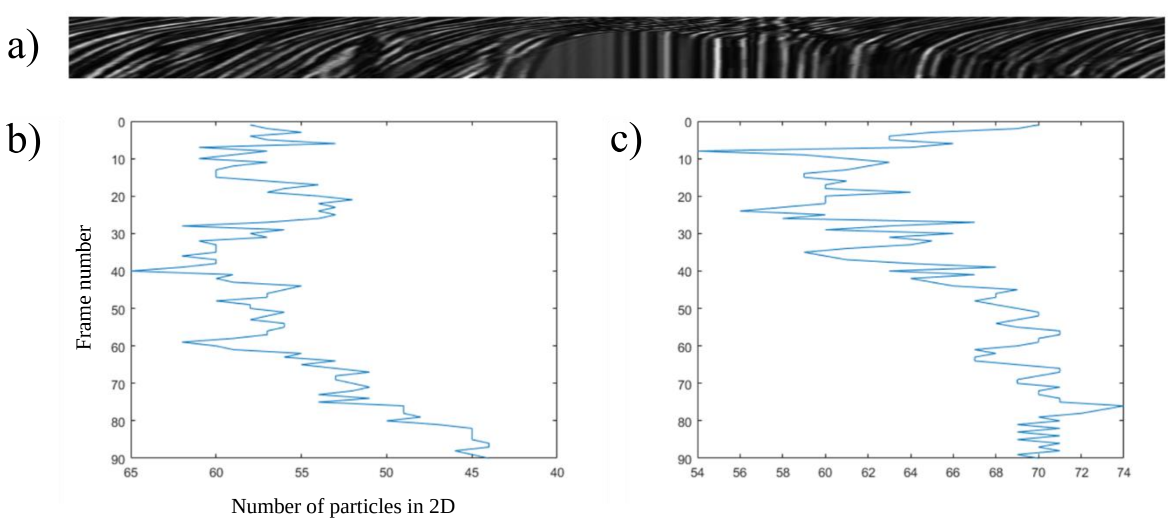

Appendix 3 Spatiotemporal diagram (a) and particle counting for left (b) and right (c) of the constriction. Individual clog formation by Raspberry-like particles with 100 nm in the microfluidic channel.

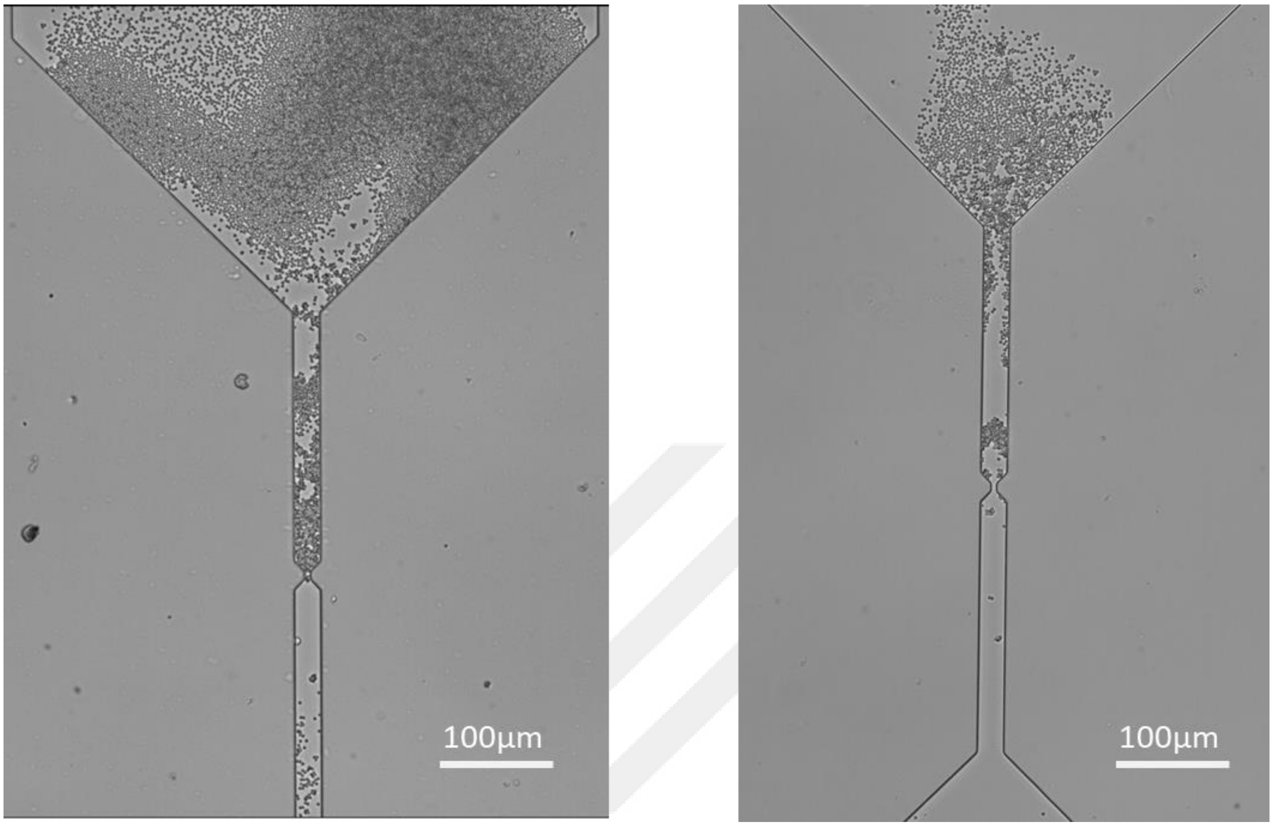

Appendix 4 Light microscope image of the constriction in the microfluidic channel showing agglomeration of raspberry-like particles with 200 nm berry particles.